



Low-cost and portable UV holographic microscope for high-contrast protein crystal imaging

Cite as: APL Photonics 4, 030804 (2019); <https://doi.org/10.1063/1.5080158>

Submitted: 06 November 2018 . Accepted: 31 January 2019 . Published Online: 01 March 2019

Mustafa Ugur Daloglu, Aniruddha Ray, Michael J. Collazo, Calvin Brown , Derek Tseng, Blanca Chocarro-Ruiz, Laura M. Lechuga, Duilio Cascio, and Aydogan Ozcan 



View Online



Export Citation



CrossMark

ARTICLES YOU MAY BE INTERESTED IN

[Adiabatic mode converters for silicon photonics: Power and polarization broadband manipulators](#)


APL Photonics 4, 030803 (2019); <https://doi.org/10.1063/1.5080247>

[Nonlinear optics in carbon nanotube, graphene, and related 2D materials](#)

APL Photonics 4, 034301 (2019); <https://doi.org/10.1063/1.5051796>

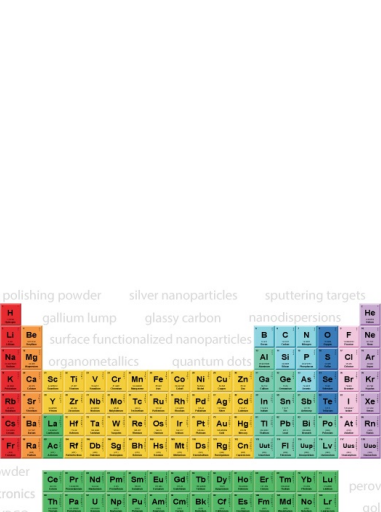
[Inter-modal Raman amplification of OAM fiber modes](#)

APL Photonics 4, 030802 (2019); <https://doi.org/10.1063/1.5051794>



AMERICAN ELEMENTS

THE ADVANCED MATERIALS MANUFACTURER®



additive manufacturing epitaxial crystal growth cerium oxide polishing powder silver nanoparticles sputtering targets III-IV semiconductors CVD precursors europium phosphors

deposition slugs OLED Lighting spintronics solar energy osmium nanoribbons thin films chalcogenides AuNPs GDC li-ion battery electrolytes 99.999% ruthenium spheres

endoheedral fullerenes copper nanoparticles diamond micropowder CIGS MBE grade materials palladium catalysts flexible electronics beta-barium borate borosilicate glass dysprosium pellets YBCO pyrolytic graphite 3d graphene foam indium tin oxide mesoporous silica raman substrates sapphire windows tungsten carbide InGaAs barium fluoride carbon nanotubes lithium niobate scandium powder

gallium lump glassy carbon nanodispersions InAs wafers laser crystals ultra high purity materials MOFs rare earth metals photovoltaics refractory metals MOCVD organometallics quantum dot superconductors transparent ceramics ultra high purity silicon

American Elements opens up a world of possibilities so you can **Now Invent!**

Over 15,000 certified high purity laboratory chemicals, metals, & advanced materials and a state-of-the-art Research Center. Printable GHS-compliant Safety Data Sheets. Thousands of new products. And much more. All on a secure multi-language 'Mobile Responsive' platform.

perovskite crystals yttrium iron garnet alternative energy h-BN gold nanocubes graphene oxide macromolecules photonics rhodium sponge fiber optics beamsplitters infrared dyes zeolites fused quartz metallocenes platinum ink buckyballs Ti-6Al-4V

Now Invent.™
The Next Generation of Material Science Catalogs

www.americanelements.com



Low-cost and portable UV holographic microscope for high-contrast protein crystal imaging

Cite as: APL Photon. 4, 030804 (2019); doi: 10.1063/1.5080158

Submitted: 6 November 2018 • Accepted: 31 January 2019 •

Published Online: 1 March 2019





View Online



Export Citation



CrossMark

Mustafa Ugur Daloglu,^{1,2,3,a)} Aniruddha Ray,^{1,2,3,b)} Michael J. Collazo,^{4,5,6,7,8,c)} Calvin Brown,^{1,2,3,d)}  Derek Tseng,^{1,2,3,e)} Blanca Chocarro-Ruiz,^{9,f)} Laura M. Lechuga,^{9,g)} Duilio Cascio,^{4,5,6,7,8,h)} and Aydogan Ozcan^{1,2,3,10,i)} 

AFFILIATIONS

¹Electrical and Computer Engineering Department, University of California, Los Angeles, California 90095, USA

²Bioengineering Department, University of California, Los Angeles, California 90095, USA

³California NanoSystems Institute (CNSI), University of California, Los Angeles, California 90095, USA

⁴Howard Hughes Medical Institute, University of California, Los Angeles, California 90024, USA

⁵Department of Energy Institute, University of California, Los Angeles, California 90024, USA

⁶Biological Chemistry Department, University of California, Los Angeles, California 90024, USA

⁷Chemistry and Biochemistry Department, University of California, Los Angeles, California 90024, USA

⁸Molecular Biology Institute, University of California, Los Angeles, California 90024, USA

⁹Catalan Institute of Nanoscience and Nanotechnology (ICN2), CSIC, BIST, and CIBER-BBN, Campus UAB, Bellaterra, 08193 Barcelona, Spain

¹⁰Department of Surgery, David Geffen School of Medicine, University of California, Engr. IV 68-119, 420 Westwood Plaza, Los Angeles, California 90095, USA

Note: This paper is part of an APL Photonics Special Topic on Computational Optical Imaging.

^{a)}mudaloglu@ucla.edu

^{b)}rayani@ucla.edu

^{c)}mcollazo@mbi.ucla.edu

^{d)}calvinbrown@g.ucla.edu

^{e)}delike@ucla.edu

^{f)}blanca.chocarro@icn2.cat

^{g)}laura.lechuga@icn2.cat

^{h)}cascio@mbi.ucla.edu

ⁱ⁾ **Author to whom correspondence should be addressed:** ozcan@ucla.edu. Tel.: +1(310)825-0915. Fax: +1(310)206-4685.

ABSTRACT

Imaging protein crystals and distinguishing them from salt crystals is an important task for protein crystallographers. The conventional tool used for this purpose is a dual-mode microscope composed of bright-field and ultraviolet (UV) induced fluorescence modes. The distinction between a protein and a salt crystal is made based upon the fluorescence response to the UV excitation, where most protein crystals absorb the UV excitation and emit fluorescence, unlike salt crystals. These dual-mode optical microscopes are sensitive; however, they are relatively bulky and expensive as they require UV-grade optics. As an alternative, here we demonstrate that on-chip UV holographic imaging offers a low-cost, portable, and robust technique to image and distinguish protein crystals from salt crystals, without the need for any expensive and bulky optical components. Only composed of a UV light-emitting-diode at 280 nm and a consumer-grade complementary metal-oxide-semiconductor image sensor de-capped and interfaced to a Raspberry Pi single-board computer, the necessary information from the crystal samples (placed very close to the sensor active area) is captured in the form of in-line holograms and extracted through digital back-propagation. In these holographic amplitude reconstructions, protein crystals appear significantly darker compared to the background due to the

strong UV absorption, unlike salt crystals which do not show any contrast, enabling us to clearly distinguish between them. We believe that the on-chip UV holographic microscope could serve as a low-cost, sensitive, and robust alternative to conventional lens-based UV-microscopes used in protein crystallography.

© 2019 Author(s). All article content, except where otherwise noted, is licensed under a Creative Commons Attribution (CC BY) license (<http://creativecommons.org/licenses/by/4.0/>). <https://doi.org/10.1063/1.5080158>

I. INTRODUCTION

Protein crystallographers rely on a dual-mode optical microscope composed of bright-field and ultraviolet (UV) induced fluorescence modes to image protein crystals as well as to distinguish them from salt crystals that could form during the crystallization process. This distinction is mainly based on the response to the UV illumination, where most protein crystals absorb the UV light and emit fluorescence through tryptophan residues, unlike most salt crystals.^{1,2} In addition to UV fluorescence,^{3,4} the strong absorption of UV light within organic materials^{5,6} has been utilized as an inherent contrast agent in imaging tissue samples,⁷ cells,⁸ intracellular nucleic acids and proteins,⁹⁻¹² viruses,¹³ and protein aggregates,¹⁴ making UV microscopy¹⁵ an important tool for researchers. However, conventional lens-based UV microscopy is a relatively expensive imaging modality, requiring the use of relatively bulky optical components that are specially designed for UV wavelengths, in addition to UV light sources and UV-sensitive cameras for bright-field imaging,² adding up to significant costs (e.g., \$35k-200k).¹⁶ Furthermore, inherent limitations of lens-based microscopy also apply to conventional UV microscopes, where the trade-off between the field-of-view (FOV) and resolution limits the total sample area that can be imaged.

As an alternative, on-chip holographic imaging¹⁷⁻²⁰ offers a cost-effective option²¹⁻²⁴ for such microscopy tasks without

the need for imaging lenses or other bulky optical components, only using consumer-grade image sensor chips²⁵ and simple light sources like light-emitting diodes (LEDs) opening up new frontiers for portability.²⁶⁻²⁹ The ever decreasing peak emission wavelengths and increasing efficiencies of LED technologies made the deep UV LEDs (240 nm-360 nm)³⁰⁻³³ more available and affordable. This, when integrated with the capabilities of portable and cost-effective on-chip holographic microscopy tools, enables a wide range of studies related to proteins, particularly in the field of crystallography.

Here we present a portable on-chip holographic imaging platform (Fig. 1) that is composed of a UV-LED operating at 280 nm peak wavelength and a de-capped complementary metal-oxide-semiconductor (CMOS) image sensor connected to a Raspberry Pi single-board computer.^{34,35} The sample is placed very close (~ 300 - $400 \mu\text{m}$) to the image sensor and the light source further above, where the interference between the light scattered from the target crystals and the background illumination creates in-line holograms that are digitized/recorded by using the image sensor. The captured frames are then digitally processed to extract the information about the target objects that is encoded in the holograms, resulting in UV transmission images over a large FOV that is only limited by the sensor active area ($>10 \text{ mm}^2$).

The utility of this platform in crystallography was demonstrated by imaging different protein crystals including proteinase K (Figs. 2 and 3), the RING1B complex (Fig. 4), maltose

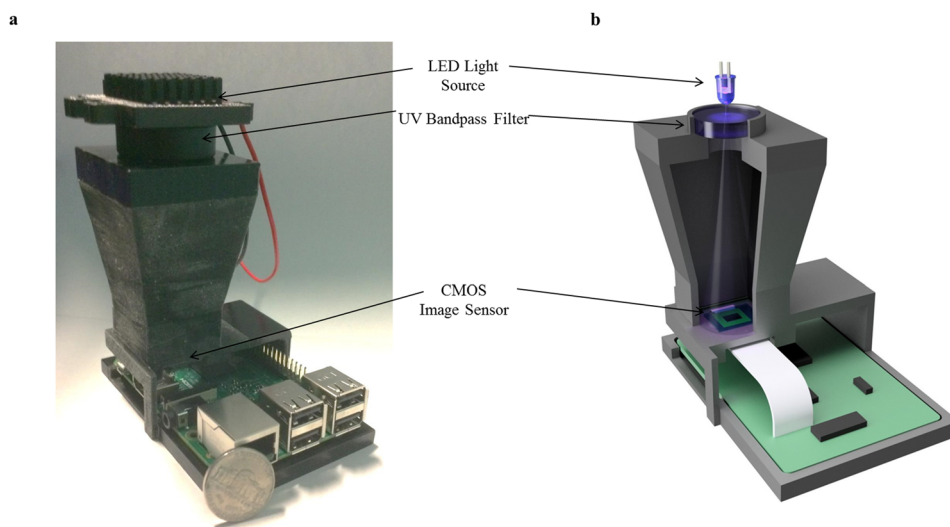


FIG. 1. (a) Our portable holographic on-chip imaging platform operates at 280 nm illumination wavelength. The UV LED is spectrally filtered using a bandpass filter to block the side-bands, letting through pure UV light with 280 nm peak wavelength and a 10 nm bandwidth toward the sample, which is placed very close to the image sensor (~ 300 - $400 \mu\text{m}$), utilizing the full active area as the imaging FOV ($>10 \text{ mm}^2$). (b) A simplified CAD model of the same portable on-chip imaging platform.

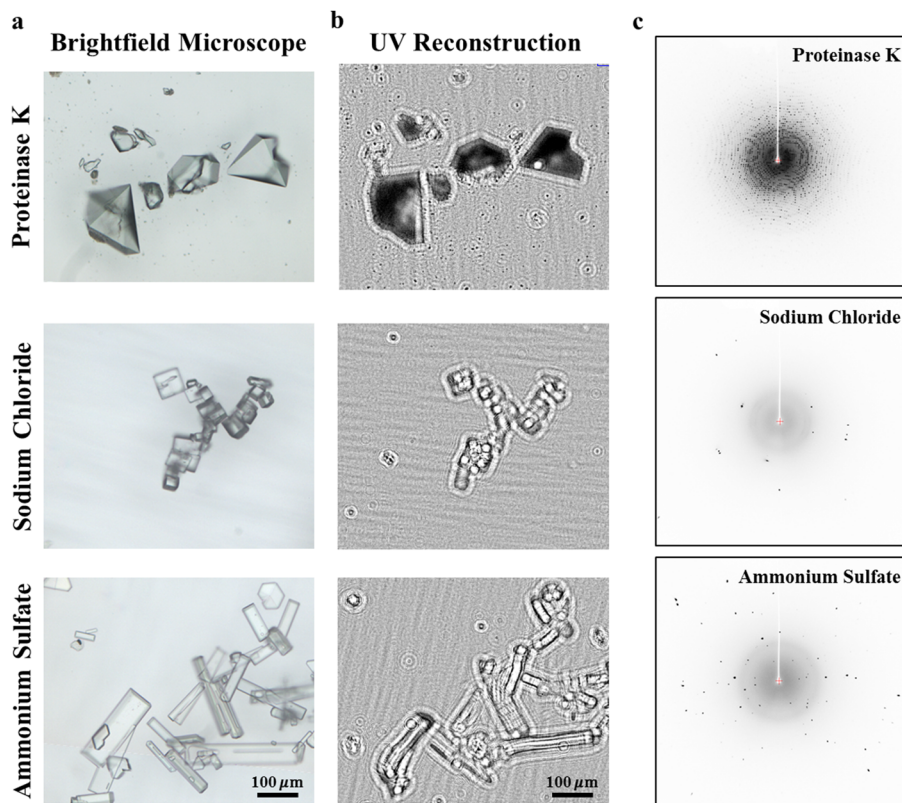


FIG. 2. Using the setup shown in Fig. 1, proteinase K crystals appear significantly darker compared to the background level due to the strong UV absorption at 280 nm, unlike salt crystals. (a) Bright-field microscope images of proteinase K, sodium chloride, and ammonium sulfate crystals. (b) Amplitude reconstructions of the same FOVs in (a), proteinase K crystals appearing significantly darker. (c) X-ray diffraction data from the proteinase K, sodium chloride, and ammonium sulfate crystal samples, with largest spacing values of 30 Å, 3.25 Å, and 3.25 Å, respectively.

binding protein (Fig. 4), and salt crystal samples which include sodium chloride (Fig. 2), ammonium sulfate (Fig. 2), lithium acetate (Fig. 3), and lithium sulfate (Fig. 3). Our mobile holographic platform can clearly differentiate between protein crystals and salt crystals due to the strong contrast in the protein crystal images which appear significantly darker compared to the background. Without the need for fine alignment and temperature stability, unlike its lens-based counterparts, this platform would be a low-cost, robust, and portable alternative to conventional UV microscopes used by protein crystallographers.

II. RESULTS AND DISCUSSION

Our portable on-chip imaging platform (Fig. 1) is built upon the versatile Raspberry Pi 3 board,³⁵ with its readily available 8 Megapixel CMOS camera, all housed within a custom designed and 3D printed shell which also holds a UV LED operating at 280 nm peak wavelength with a band-pass filter to block the side-band emissions.^{31,32,36} The CMOS camera is de-capped, removing the lens module, and the sample is placed very close ($\sim 300\text{-}400\ \mu\text{m}$) to the active area of the image sensor chip that is fully utilized as the imaging FOV [$>10\ \text{mm}^2$, Fig. 3(a)]. The filtered UV light is scattered through the sample, generating in-line holograms through its interference with the background light that is captured by using the

image sensor. These holographic images are then digitally processed to extract the amplitude information encoded in the interference patterns from the target objects.

We tested our portable on-chip imaging platform to verify the effect of strong UV absorption in our amplitude reconstructions, imaging protein crystals (Fig. 2). Samples were prepared by constructing imaging chambers using UV fused silica glass slides and pieces of ACLAR protein crystallization covers, a standard material used by protein crystallographers which is also UV transparent. It is important to note that additional consideration has to be given in the transparency of materials for coherent imaging modalities like holography, as the irregularities in the material volume could result in strong background distortions. The standard UV transparent ACLAR used by protein crystallographers is suitable for holographic imaging, only creating a faint modulation in the background [Fig. 2(b)] which does not affect our imaging quality.

Our imaging platform (Fig. 1) was first tested by preparing a sample with proteinase K, a serine protease readily available for crystallization, which contains aromatic amino acids that fluoresce when excited at 280 nm light, and two salt crystal samples (sodium chloride and ammonium sulfate) [Figs. 2(a) and 2(b)], where the respective X-ray diffraction data are shown in Fig. 2(c). Individual crystals were pipetted along with $\sim 1\ \mu\text{l}$ of solution onto the ACLAR piece (sticky side facing up), and a UV fused silica was used to seal the droplet

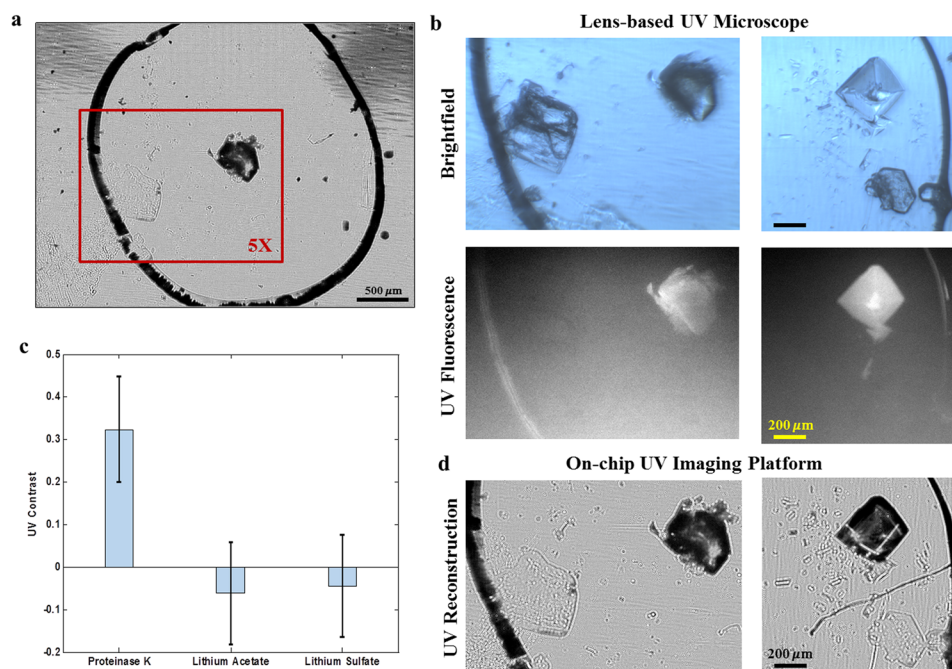


FIG. 3. A low-cost, portable, and high-throughput alternative to lens-based UV microscopes used by protein crystallographers to distinguish between protein and salt crystals. (a) The full FOV ($>10 \text{ mm}^2$) image captured by our on-chip microscopy platform (Fig. 1) where the red rectangle shows a typical FOV possible using a lens-based UV microscope with a 5× objective lens. (b) Samples containing proteinase K and salt crystals (lithium acetate and lithium sulfate) in the same chamber, imaged by using the lens-based UV microscope in both brightfield and UV fluorescence modes. The proteinase K crystals strongly absorb the 280 nm UV light and emit fluorescence, where the salt crystals do not. (c) Protein crystals show a significantly stronger contrast compared to salt crystals ($p < 0.02$). The standard deviation bars represent the variation of the contrast within the rectangular regions used to calculate the average contrast of the target objects. (d) The amplitude reconstructions of the same FOVs captured by our on-chip UV imaging platform. The same crystals that emitted fluorescence in (b) appear significantly darker compared to the background due to the stronger absorption, while the crystals that did not emit fluorescence do not show statistically significant contrast in our amplitude reconstructions.

into the chamber. The amplitude reconstructions of our holograms clearly show that the protein crystals appear much darker compared to the background, unlike the salt crystals [Fig. 2(b)]. The amplitude reconstruction results shown in Fig. 2(b) could be further improved using various phase-retrieval techniques¹⁷ to mitigate twin-image artifacts, at the cost of additional computation and/or holographic measurements.

To further evaluate our portable on-chip holographic imaging platform, we imaged mixed-samples containing both protein (proteinase K) and salt crystals (lithium acetate and lithium sulfate) within the same FOV [Figs. 3(a), 3(b), and 3(d)], prepared by sandwiching droplets of $\sim 1 \mu\text{l}$ buffer solution containing the crystals between a UV fused silica slide and a piece of ACLAR sheet. The crystals were grown in their respective buffer solutions and then individually fished by a microloop and deposited in the droplet before sealing. The samples were first imaged with the lens-based microscope, which is able to distinguish between the protein and the salt crystal through the fluorescence of the protein crystal [Fig. 3(b)], where the protein crystal is observed to be emitting fluorescence, while the salt crystal remains dark. The samples were then imaged with our on-chip microscopy platform [Figs. 3(a) and 3(d)], where the proteinase K crystals showed a

significantly stronger contrast ($p < 0.02$) compared to the salt crystals [Fig. 3(c)]. We calculated the contrast (C) in our UV holographic amplitude reconstructions by subtracting the average amplitude signal of the target crystals (S_c) from the average background signal value (S_b) and dividing this difference by the average background signal value,^{14,37} i.e.,

$$C = \frac{S_b - S_c}{S_b}, \quad (1)$$

where S_c is calculated within the largest rectangular region that fits inside the target crystal and S_b is calculated within a clear region of the FOV that does not contain any objects.

To further test the imaging capabilities of our portable on-chip holographic imaging platform for protein crystallography, additional experiments were performed using (1) the RING1B complex, which is associated with the nuclear membrane and participates in histone ubiquitination in humans,³⁸ and (2) the maltose binding protein, which breaks down maltodextrins in *Escherichia coli* and also forms UV active crystals³⁹ (Fig. 4). All the samples under test were imaged by using the lens-based UV microscope first and then by using our on-chip UV microscope [Fig. 4(a)]. The capabilities of our portable UV imaging platform in distinguishing between protein and salt crystals were further verified with these different types

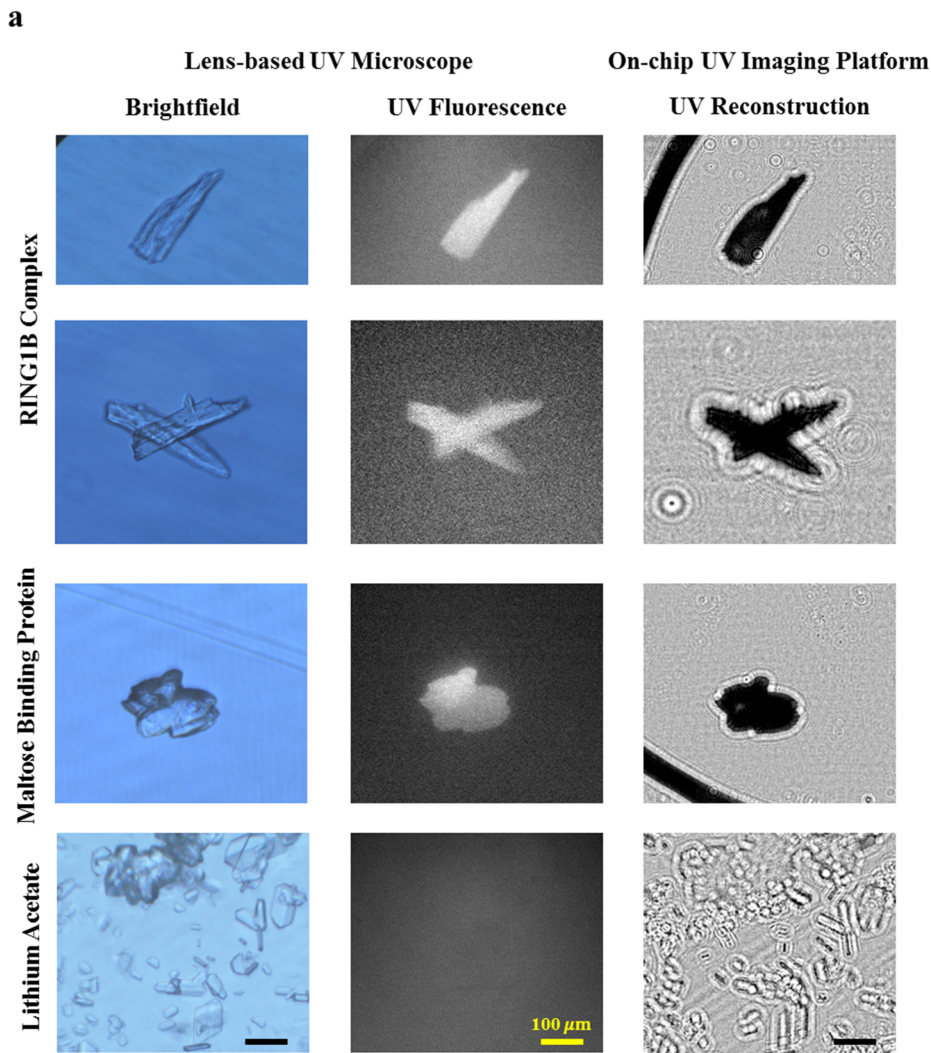
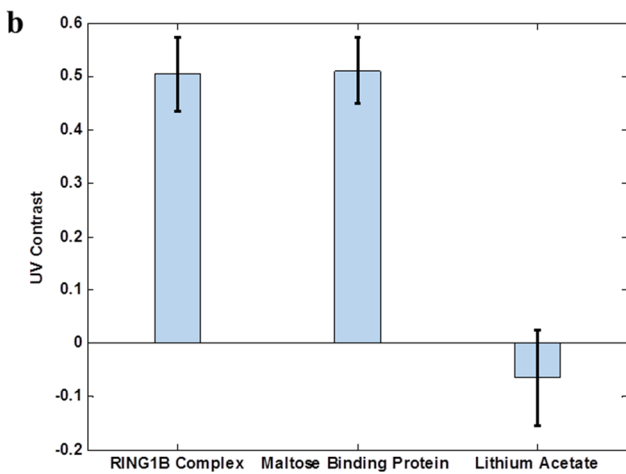


FIG. 4. High contrast imaging capabilities of our portable on-chip holographic imaging platform further demonstrated by imaging RING1B complex and maltose binding protein crystals, where lithium acetate crystals were used as control. (a) The protein crystals showed fluorescence when imaged by the lens-based UV imaging platform, while the salt crystals did not show any significant fluorescence. In the same manner, amplitude reconstructions of the protein crystals showed a significant contrast, while the salt crystals did not. (b) This significant contrast difference ($p < 0.003$) clearly shows the efficacy of the on-chip UV imaging platform in differentiating protein crystals from salt crystals. The standard deviation bars represent the variation of the contrast within the rectangular regions used to calculate the average contrast of the target objects.



of proteins, which showed a significantly higher contrast ($p < 0.003$) compared to salt crystals [Fig. 4(b)].

In summary, recent improvements in UV LED technologies have made deep UV LEDs with short peak emission wavelengths and improved efficiencies more accessible, enabling the design of a portable and low-cost on-chip UV imaging platform as a potential alternative to the expensive and bulky dual-mode UV microscopes used by protein crystallographers. We expect that our portable on-chip UV holographic imaging platform could be even further strengthened with near real-time imaging capabilities, driven by future improvements in deep UV LED power output efficiencies, enabling the use of lower sensor integration times and the increasing availability of embedded graphics processing units (GPUs) for single-board computers.

III. MATERIALS AND METHODS

A. UV on-chip imaging platform

Our portable on-chip microscopy platform (Fig. 1) is composed of a de-capped 8 Mega-pixel (3280 horizontal \times 2464 vertical, with an active area of $\sim 10.14 \text{ mm}^2$), $1.12 \mu\text{m}$ pixel pitch, CMOS image sensor (IMX219, Sony Corporation, Tokyo, Japan) interfaced to a Raspberry Pi 3B single-board computer, a deep UV LED operating at 280 nm peak wavelength (TH-UV280J9-C-H-B, Tianhui Optoelectronics Co., Ltd, Guangdong Province, China), and a UV band-pass filter with a center wavelength of 280 nm and a bandwidth of 10 nm (FF01-280/10-25, Semrock, NY, USA) to block the side-band emissions^{31,32,36} from the UV LED. All of these components are housed within a custom designed and 3D printed acrylonitrile butadiene styrene (ABS) (Stratasys, Dimension Elite) shell. A custom Python script was used to capture, extract, and save the raw frames/holograms from the sensor to the onboard storage of the Raspberry Pi 3B.

B. Data processing

Since the green pixels of the image sensor were most responsive to the UV illumination,¹⁴ the values in the red and blue pixels of the raw frames were replaced with the average of their neighboring green pixels. The frames containing holographic projections were then digitally back-propagated using the angular spectrum approach,⁴⁰ numerically solving the Rayleigh-Sommerfeld integral by multiplying the Fourier transform of the hologram with the transfer function of wave propagation,^{17,26} generating the amplitude images of the sample. The complete data processing takes ~ 1 minute using a standard desktop computer (Dell Optiplex 9010, Intel i7, 32 GB RAM) operating MATLAB (MathWorks, MI, USA).

The statistical significance of the increased contrast in the amplitude reconstructions of protein crystals compared to salt crystals was verified using a t-test⁴¹ with two separate experiments for proteinase K [Fig. 3(d)] and three separate experiments for the additional set of proteins which included the RING1B complex and the maltose binding protein [Fig. 4(a)].

C. Sample preparation

UV compatible materials which include UV fused silica slides (10 mm \times 10 mm, 0.2 mm thick, MTI Corp., CA, USA) and pieces of standard protein crystallization covers made of ACLAR composed of poly-chloro-trifluoroethylene (Grace Bio-Labs ProCrystal Cover 875238, OR, USA) were used to construct the sample chambers holding the crystal samples. A 0.8–1 μl droplet containing the crystals and the corresponding buffer solution was deposited onto an ACLAR piece containing one well, sticky side facing up. A UV fused silica slide was then gently used to cover the well, sealing the droplet. It is noteworthy that the ACLAR standard protein crystallization cover material was suitable for coherent imaging and only resulted in a faint background modulation [Fig. 2(b)] which did not affect our imaging quality.

D. Protein and salt crystallization

A TTP LabTech mosquito (TTP Labtech, Inc., MA, USA) was used to generate 96-well hanging drop crystallization setups. All protein crystals were grown in a manner of days using vapor diffusion. Proteinase K (VWR catalog number 97062-238, PA, USA) was crystallized by dissolving lyophilized powder in water to obtain a 50 mg/ml stock. The stock solution was mixed 1:1 with 1.5 M ammonium sulfate and 0.1 M Tris-HCl pH 7.5. Maltose binding protein 80 mg/ml in 20 mM Tris-HCl pH 8.0 and 50 mM NaCl was crystallized by mixing 1:1 with 0.2M magnesium chloride hexahydrate, 0.1M 4-Morpholineethanesulfonic acid pH 6.0%, and 20% w/v Polyethylene glycol 6000. Oligomerization regions of RING1B, polycomb group RING finger protein 4, chromobox 8, and polyhomeotic homolog 1 were supplied by the Chemistry and Biochemistry Department at UCLA. This sample was mixed 1:1 with 0.7M sodium formate pH 7.0% and 20% w/v PEG 3350. All 300 nl drops were equilibrated over 100 μl of the corresponding crystallization solutions.

1.0M sodium chloride, 2.0M ammonium sulfate, 1.0M lithium acetate, and 1.0 lithium sulfate were dispensed in μl aliquots and allowed to evaporate in air while being observed in a stereomicroscope. Crystals that formed by dehydration in aqueous solution were manually harvested using 50 μm microloops (Mitegen M5-L18SP-50LD, NY, USA) and placed in 1 μl of the stock salt solution. These solutions, containing crystals, were placed on the ACLAR surface by using a pipette for imaging.

E. Lens-based UV microscopy

A dual-mode UV microscope (Korima PRS-1000, CA, USA) was used for comparison with the holographic imaging platform. Samples were imaged with the UV microscope first and then holographically imaged with our mobile instrument. Crystals were exposed to 280 nm light for no more than 5 s, and the images taken were compared with the corresponding holographic images [Fig. 4(a)].

F. X-ray diffraction

To further distinguish protein crystals from salt, diffraction images were taken. Individual crystals from the target

sample were harvested and placed in their mother liquor with 33% glycol added to resist the formation of crystalline water. A rotating anode generator (Rigaku FRE+, Tokyo, Japan) and an imaging plate detector (Rigaku HTC, Tokyo, Japan) were employed for X-ray data collection. Macromolecule crystals are distinguishable from salt crystals by lower resolution reflections that occur as the result of larger spacing between symmetric elements of the crystal [Fig. 2(c)].

IV. CONCLUSIONS

We designed and built a low-cost and portable on-chip holographic imaging platform operating at the deep UV wavelength of 280 nm for high-contrast imaging of protein crystals. Without the need for sensitive, bulky, and costly components, our platform offers a low-cost, high-throughput, and robust alternative to the dual-mode optical microscopes composed of bright-field and ultraviolet (UV) induced fluorescence modes that are routinely used by protein crystallographers to image protein crystals and to distinguish them from salt crystals. We tested the on-chip holographic imaging platform by imaging different protein crystals including proteinase K, maltose binding protein, and the RING1B complex in comparison with several different salt crystals which include sodium chloride, ammonium sulfate, lithium acetate, and lithium sulfate. While the amplitude reconstructions of the protein crystals appear much darker compared to the background, the salt crystals do not show any contrast, clearly distinguishing between the two types of crystals. We believe that our portable on-chip holographic platform could aid protein crystallographers as a low-cost and robust alternative platform to image protein crystals and to distinguish them from salt crystals.

ACKNOWLEDGMENTS

The Ozcan Research Group at UCLA acknowledges the support of NSF Engineering Research Center (ERC, PATHS-UP), the Army Research Office (ARO; Nos. W911NF-13-1-0419 and W911NF-13-1-0197), the ARO Life Sciences Division, the National Science Foundation (NSF) CBET Division Biophotonics Program, the NSF Emerging Frontiers in Research and Innovation (EFRI) Award, the NSF INSPIRE Award, NSF Partnerships for Innovation: Building Innovation Capacity (PFI:BIC) Program, the National Institutes of Health (NIH, No. R21EB023115), the Howard Hughes Medical Institute (HHMI), Vodafone Americas Foundation, the Mary Kay Foundation, and the Steven and Alexandra Cohen Foundation. The authors acknowledge Zachary Scott Ballard and Yichen Wu for their help in obtaining some of the hardware components. We thank Isaijah Johnson and Trevor Sobol for their assistance in crystallizing protein samples for evaluation. The UCLA X-ray diffraction facilities are supported by the BER program of the Department of Energy Office of Science under Award No. DE-FC02-02ER63421.

A.O. is the co-founder of a company that commercializes computational imaging and sensing technologies.

REFERENCES

- ¹S. Desbois, S. A. Seabrook, and J. Newman, "Some practical guidelines for UV imaging in the protein crystallization laboratory," *Acta Crystallogr., Sect. F: Struct. Biol. Cryst. Commun.* **69**, 201–208 (2013).
- ²C. S. Lunde et al., "UV microscopy at 280 nm is effective in screening for the growth of protein microcrystals," *J. Appl. Crystallogr.* **38**, 1031–1034 (2005).
- ³I. Vayá, T. Gustavsson, F.-A. Miannay, T. Douki, and D. Markovitsi, "Fluorescence of natural DNA: From the femtosecond to the nanosecond time scales," *J. Am. Chem. Soc.* **132**, 11834–11835 (2010).
- ⁴Hargis, Jr. et al., "Ultraviolet fluorescence identification of protein, DNA, and bacteria," *Proc. SPIE* **2366**, 147 (1995).
- ⁵Y. Kumamoto, "Deep-ultraviolet microscopy and microspectroscopy," in *Far- and Deep-Ultraviolet Spectroscopy*, edited by Y. Ozaki and S. Kawata (Springer, Japan, 2015), pp. 123–144.
- ⁶F.-X. Schmid, *Biological Macromolecules: UV-Visible Spectrophotometry* (eLS, 2001).
- ⁷E. H. Land et al., "A color translating ultraviolet microscope," *Science* **109**, 371–374 (1949).
- ⁸J. R. G. Bradfield and M. Errera, "Ultra-violet absorption of living cells," *Nature* **164**, 532–533 (1949).
- ⁹D.-K. Yao, K. Maslov, K. K. Shung, Q. Zhou, and L. V. Wang, "In vivo label-free photoacoustic microscopy of cell nuclei by excitation of DNA and RNA," *Opt. Lett.* **35**, 4139–4141 (2010).
- ¹⁰B. J. Zeskind et al., "Nucleic acid and protein mass mapping by live-cell deep-ultraviolet microscopy," *Nat. Methods* **4**, 567–569 (2007).
- ¹¹M. C. Cheung, J. G. Evans, B. McKenna, and D. J. Ehrlich, "Deep ultraviolet mapping of intracellular protein and nucleic acid in femtograms per pixel," *Cytometry, Part A* **79A**, 920–932 (2011).
- ¹²M. C. Cheung et al., "Intracellular protein and nucleic acid measured in eight cell types using deep-ultraviolet mass mapping," *Cytometry, Part A* **83A**, 540–551 (2013).
- ¹³J. E. Barnard, "Microscopical evidence of the existence of saprophytic viruses," *Br. J. Exp. Pathol.* **16**, 129 (1935).
- ¹⁴M. U. Daloglu et al., "Computational on-chip imaging of nanoparticles and biomolecules using ultraviolet light," *Sci. Rep.* **7**, 44157 (2017).
- ¹⁵J. Smiles, "Ultraviolet microscopy," *J. Appl. Bacteriol.* **21**, 137–142 (1958).
- ¹⁶H. S. Gill, "Evaluating the efficacy of tryptophan fluorescence and absorbance as a selection tool for identifying protein crystals," *Acta Crystallogr., Sect. F: Struct. Biol. Cryst. Commun.* **66**, 364–372 (2010).
- ¹⁷Z. Gorocs and A. Ozcan, "On-chip biomedical imaging," *IEEE Rev. Biomed. Eng.* **6**, 29–46 (2013).
- ¹⁸A. Greenbaum et al., "Imaging without lenses: Achievements and remaining challenges of wide-field on-chip microscopy," *Nat. Methods* **9**, 889–895 (2012).
- ¹⁹D. Tseng et al., "Lensfree microscopy on a cellphone," *Lab Chip* **10**, 1787 (2010).
- ²⁰W. Luo, A. Greenbaum, Y. Zhang, and A. Ozcan, "Synthetic aperture-based on-chip microscopy," *Light Sci. Appl.* **4**, e261 (2015).
- ²¹E. McLeod and A. Ozcan, "Unconventional methods of imaging: Computational microscopy and compact implementations," *Rep. Prog. Phys.* **79**, 076001 (2016).
- ²²E. McLeod and A. Ozcan, "Microscopy without lenses," *Phys. Today* **70**(9), 50–56 (2017).
- ²³A. Ozcan and E. McLeod, "Lensless imaging and sensing," *Annu. Rev. Biomed. Eng.* **18**, 77–102 (2016).
- ²⁴E. McLeod, Q. Wei, and A. Ozcan, "Democratization of nanoscale imaging and sensing tools using photonics," *Anal. Chem.* **87**, 6434–6445 (2015).
- ²⁵J. C. Contreras-Naranjo, Q. Wei, and A. Ozcan, "Mobile phone-based microscopy, sensing, and diagnostics," *IEEE J. Sel. Top. Quantum Electron.* **22**, 1–14 (2016).
- ²⁶O. Mudanyali et al., "Compact, light-weight and cost-effective microscope based on lensless incoherent holography for telemedicine applications," *Lab Chip* **10**, 1417 (2010).

- ²⁷O. Mudanyali, C. Oztoprak, D. Tseng, A. Erlinger, and A. Ozcan, "Detection of waterborne parasites using field-portable and cost-effective lensfree microscopy," *Lab Chip* **10**, 2419 (2010).
- ²⁸T.-W. Su, A. Erlinger, D. Tseng, and A. Ozcan, "Compact and light-weight automated semen analysis platform using lensfree on-chip microscopy," *Anal. Chem.* **82**, 8307–8312 (2010).
- ²⁹A. Feizi *et al.*, "Rapid, portable and cost-effective yeast cell viability and concentration analysis using lensfree on-chip microscopy and machine learning," *Lab Chip* **16**, 4350–4358 (2016).
- ³⁰L. Krčmová *et al.*, "Deep-UV-LEDs in photometric detection: A 255 nm LED on-capillary detector in capillary electrophoresis," *Analyst* **134**, 2394 (2009).
- ³¹K. G. Kraiczek, R. Bonjour, Y. Salvadé, and R. Zengerle, "Highly flexible UV-vis radiation sources and novel detection schemes for spectrophotometric HPLC detection," *Anal. Chem.* **86**, 1146–1152 (2014).
- ³²M. S. Shur and R. Gaska, "III-nitride based deep ultraviolet light sources," *Proc. SPIE* **6894**, 689419 (2008).
- ³³Y. Li, P. N. Nesterenko, B. Paull, R. Stanley, and M. Macka, "Performance of a new 235 nm UV-LED-Based on-capillary photometric detector," *Anal. Chem.* **88**, 12116–12121 (2016).
- ³⁴Y.-C. Wu *et al.*, "Air quality monitoring using mobile microscopy and machine learning," *Light Sci. Appl.* **6**, e17046 (2017).
- ³⁵C Edwards, "Not-so-humble Raspberry Pi gets big ideas," *Eng. Technol.* **8**, 30–33 (2013).
- ³⁶J.-S. Park *et al.*, "Origins of parasitic emissions from 353 nm AlGaIn-based ultraviolet light emitting diodes over SiC substrates," *Jpn. J. Appl. Phys., Part 2* **45**, 4083–4086 (2006).
- ³⁷B. Yuan *et al.*, "A system for high-resolution depth-resolved optical imaging of fluorescence and absorption contrast," *Rev. Sci. Instrum.* **80**, 043706 (2009).
- ³⁸R. Eskeland *et al.*, "Ring1B compacts chromatin structure and represses gene expression independent of histone ubiquitination," *Mol. Cell* **38**, 452–464 (2010).
- ³⁹O. K. Kellermann and T. Ferenci, "[75] Maltose-binding protein from *Escherichia coli*," in *Methods in Enzymology* (Elsevier, 1982), Vol. 90, pp. 459–463.
- ⁴⁰J. W. Goodman, *Introduction to Fourier Optics* (Roberts & Co., 2005).
- ⁴¹D. S. Fay, "A biologist's guide to statistical thinking and analysis," *Worm-Book* **2013**, 1–54.